2023-04-20

Monte Carlo generation of localised particle trajectories

Ahumada, I

10.1103/PhysRevE.00.005300
Physical review E: Statistical, nonlinear, biological, and soft matter physics
American Physical Society

Supplementary Material: Monte Carlo generation of localised particle trajectories

Ivan Ahumada*
Instituto de Física y Matemáticas,
Universidad Michoacana de San Nicolás de Hidalgo, Morelia, México.

James P. Edwards†
Centre for Mathematical Sciences, University of Plymouth, Plymouth, PL4 8AA, UK

I. PATH AVERAGED POTENTIALS

Here we report the functional forms of the path averaged potential first studied in [1]. For the linear potential, $V(x) = kx$, the PAP can be determined analytically and is Gaussian,

$$\wp(v|y,x;T) = \sqrt{\frac{6}{\pi k^2 T^3}}\mathrm{e}^{-\frac{3}{2T}(x+y)^2}\mathrm{e}^{-\frac{6}{k^2T^3}\left(v^2-kT(x+y)v\right)} = \sqrt{\frac{6}{\pi k^2 T^3}}\mathrm{e}^{-\frac{6}{k^2T^3}\left(v-\frac{kT}{2}(x+y)\right)^2}. \tag{1}$$

Note that $\int_\infty^\infty dv\,\wp(v|y,x;T) = 1$ and that $\wp(v|y,x;T)$ satisfies the boundary conditions $\lim_{T\to 0}\wp(v|y,x;T) = \lim_{k\to 0}\wp(v|y,x;T) = \delta(v)$, which is the free particle limit.

A spectral representation of the PAP for the harmonic oscillator, $V(x) = \frac{1}{2}m\omega^2x^2$, is given (for $x = y = 0$, sufficient for this work) in their equation (33) which we can simplify a small amount to

$$\wp(v|y,x;T) = 32\Theta(v)\sqrt{\frac{\omega T}{\pi^2}}\sum_{n\ \text{even}}\frac{n!\,v_n^{\frac{3}{2}}\,\mathrm{e}^{-v_n}}{2^{n+\frac{1}{2}}(\frac{n}{2})!^2\left((n+\frac{1}{2})\omega T\right)^{\frac{5}{2}}}\left[\left(v_n-\frac{3}{4}\right)K_{\frac{1}{4}}(v_n)+v_nK_{\frac{5}{4}}(v_n)\right], \tag{2}$$

where $v_n = \frac{\left[\left(n+\frac{1}{2}\right)\omega T\right]^2}{8v}$ and the K_α are the modified Bessel functions of the second kind. The series converges very rapidly and can be truncated at n as small as 10 without sacrificing precision. This function satisfies the same normalisation and boundary condition in the limit of vanishing coupling, ω. Both functions can therefore be interpreted as probability distributions for the Wilson line variable, v, on the space of Brownian motion trajectories. They measure the relative contribution to the path integral of trajectories whose Wilson line variable evaluates to a the given value, v. The kernel is obtained by integrating this over v with Gaussian weight (see Main Text).

As described in the Main Text, a good sampling of the path integral equates to generating trajectories such that the values of their associated Wilson lines sample well the $\wp$ appropriate to the system. Much of the work in the main text is completed in this "v-space" which provides insight in a similar way to how Fourier (momentum) space can complement working in position space.

A. Numerical analysis of trajectories and distributions

The distributions (1) and (2) were corroborated numerically in [1, 2]. Here we provide analogous numerical confirmation of the "shifted distributions" denoted by $\wp_\Omega(v)$ and $\wp_\kappa(v)$ in section III of the Main Text – see equations (22-23). These also allow us to obtain the distributions $\wp'(v)$ and $\wp''(v)$ satisfied by the shifted variables, $\{v_i'\}$ and $\{v_i''\}$ in the Main Text – equations (26) and (30). The shifted distributions can be found by using the Fourier representation of the δ-function or by noting that the constraint ensures that

$$\frac{1}{K_\bullet}\int\mathscr{D}x(\tau)\,\delta\big(v-v[x]\big)\,\mathrm{e}^{-\int_0^T d\tau\left[\frac{m\dot{x}^2}{2}+U_\bullet(x)\right]} = \frac{K_0}{K_\bullet}\mathrm{e}^{-(U_\bullet/V)v}. \tag{3}$$

We begin by showing how the spatial distribution of trajectories changes when the background potentials are present, using simulations in two dimensional quantum mechanics for illustrative convenience. The harmonic oscillator

* ivan.ahumada@umich.mx (Corresponding Author)
† james.p.edwards@plymouth.ac.uk

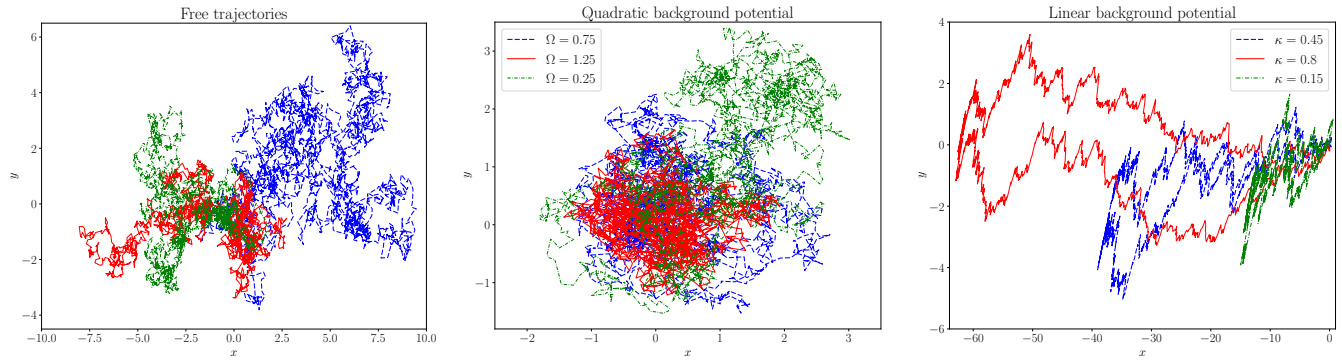

FIG. 1. Comparison of trajectories generated using standard WMC (left panel) and including background potentials. Middle panel: $U_\Omega(x) = \frac{1}{2}m\Omega^2x^2$ for $\Omega = 0.25$ (upper-most dashdotted green line), $\Omega = 0.75$ (central dashed blue line) and $\Omega = 1.25$ (left-most solid red line), $m = 1$ and $T = 20$. Right panel: for $U_\kappa(x) = \kappa x$ we used $\kappa = 0.15$ (right-most dashdotted green line), $\kappa = 0.45$ (central dashed blue line) and $\kappa = 0.8$ (far left solid red line), $m = 1$ and $T = 25$. Free trajectories were generated with $m = 1$ at $T = 30$. All simulations used $N_p = 2048$ points per loop for each plot. The influence of the backgrounds on the spatial extent of trajectories is clear (note the differing scales on the axes).

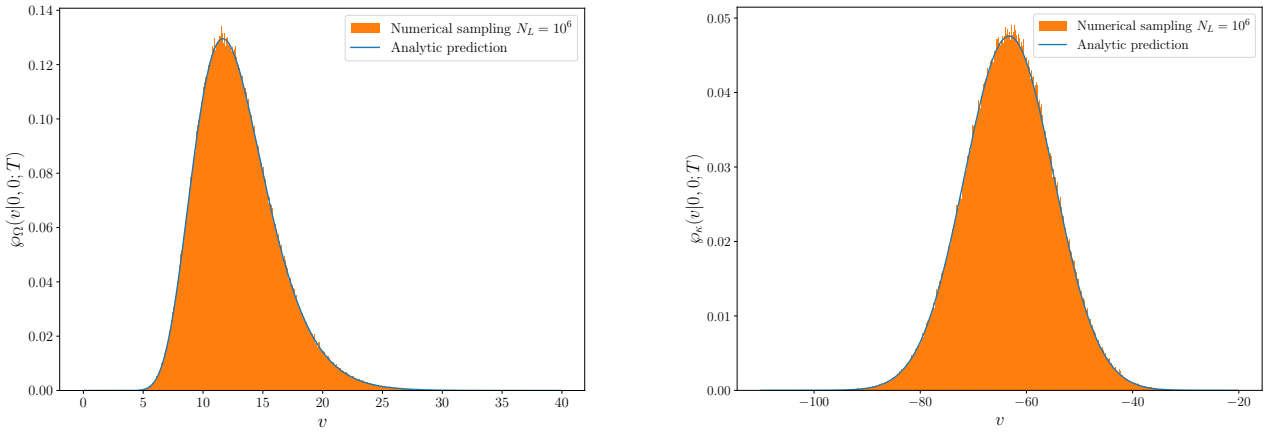

FIG. 2. Numerical corroboration of the shifted distributions $\wp_\Omega(v)$ for $\Omega = 0.75$ and $m = 1$, $\omega = 1$, $T = 40$, and $\wp_\kappa(v)$ for $\kappa = 0.45$, and $m = 1$, $k = 0.5$, $T = 15$, using $N_L = 10^6$ trajectories. The blue solid lines represent the analytical results from the Main Text. The small deviations are statistical fluctuations that can be reduced by increasing N_L and N_P.

background should concentrate trajectories about its minimum, here taken to be the origin. The linear background (with respect to one dimension, x say) will be seen to push trajectories towards smaller values of x. In Figure 1 we contrast trajectories generated with standard WMC (no background) and in the presence of the harmonic oscillator and linear potentials using the algorithms provided in Appendix A of the Main Text.

The effect of the adjusted spatial growth of the trajectories on values taken by the Wilson line variables can be seen in Figures 2–3, where we show numerical estimation of the distributions on these values against the analytically determined distributions. The numerical estimation is carried out by generating a number, N_L, of trajectories according to the algorithms provided in Appendix A of the Main Text, which produce a set of values $\{v_i\}_{i=1}^{N_L}$ of the Wilson line variables of each trajectory. These are then placed into bins to form a density-histogram, which is compared against the functions determined analytically in the Main Text.

The figures show that the Wilson line variables are providing good samples of the PAP in question, which confirm the correctness of the algorithms for generating trajectories reported in the Main Text. Moreover, comparing these to the "un-shifted" PAP (denoted $\wp(v)$ for both systems), it is apparent that the modified distributions favour *smaller* values of v. Now, since the kernel is constructed according to equation (12), trajectories with smaller v dominate its determination. Hence it can be seen that the background is simply concentrating the trajectories to regions that better sample the potential of the systems (in the spirit of importance sampling). As proved in the Main Text, the

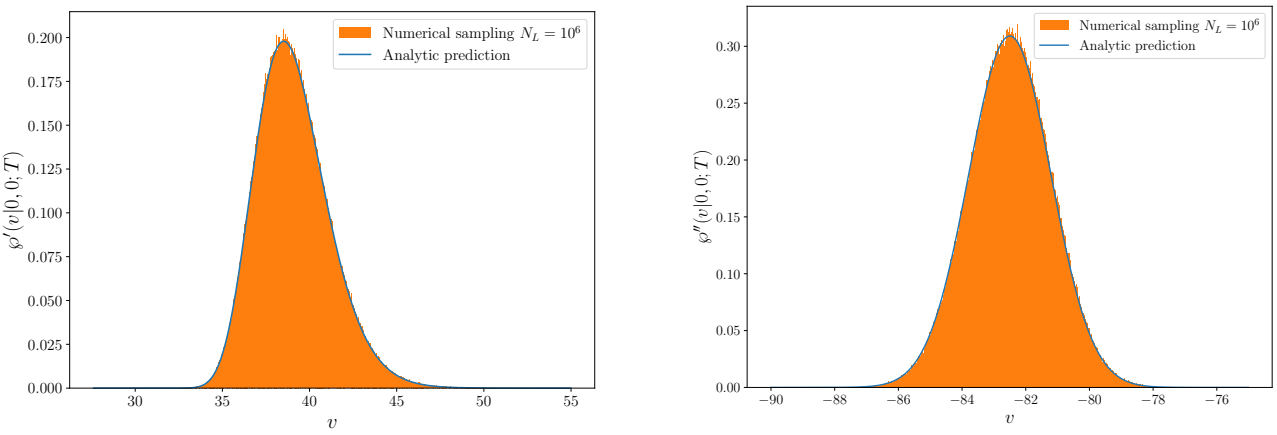

FIG. 3. Numerical corroboration of the shifted distributions $\wp'(v)$, for $\Omega = 0.75$ and $m = 1$, $\omega = 1$, $T = 80$, and $\wp''(v)$, for $\kappa = 0.45$, and $m = 1$, $k = 0.5$, $T = 20$, using $N_L = 10^6$ trajectories. The blue solid lines represent the analytical results from the Main Text.

bias from doing this is removed by the compensation factors which ensure a faithful reconstruction of the propagator, but by having favoured trajectories that better sample the potential, the undersampling problem is mitigated.

1. *Compensating potentials*

For systems where the PAP is not known in closed form (e.g. when (12) of the Main Text cannot be evaluated analytically), the compensation factors that ensure the kernel is correctly recovered are unknown. However, the Main Text shows how the bias introduced by the modified algorithms can be removed by subtracting the effects of the background potential directly in the path integral. Figure 4 demonstrates the numerical sampling of the distributions $\widetilde{\wp}(v)$ and $\widehat{\wp}(v)$ defined in the Main Text, which are distributions on the Wilson line variable for the modified potential.

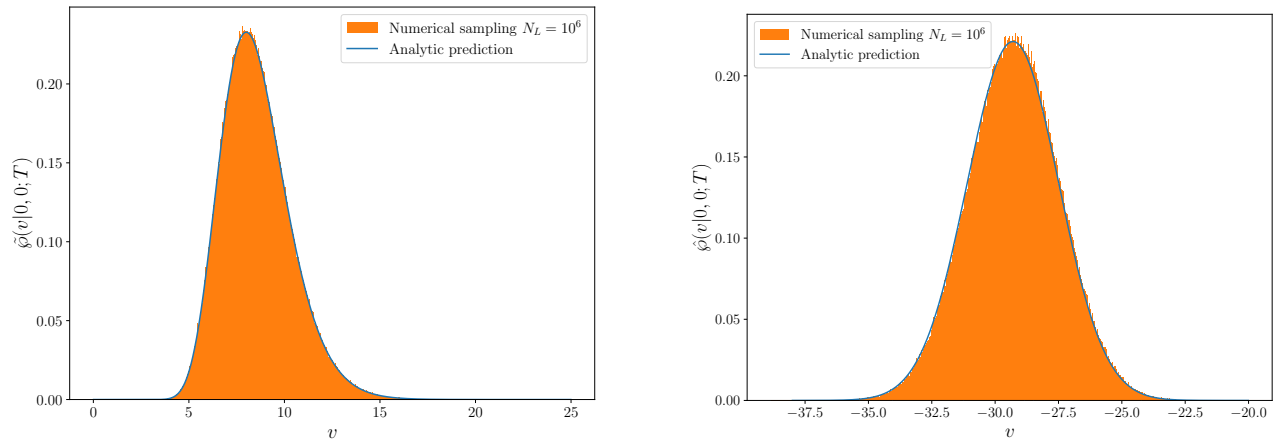

FIG. 4. Numerical corroboration of the shifted distributions $\widetilde{\wp}(v)$ for $\Omega = 0.75$ and $m = 1$, $\omega = 1$, $T = 60$, and $\widehat{\wp}(v)$ for $\kappa = 0.45$, and $m = 1$, $k = 0.5$, $T = 25$, using $N_L = 10^6$ trajectories. The blue solid lines represent the analytical results from the Main Text.

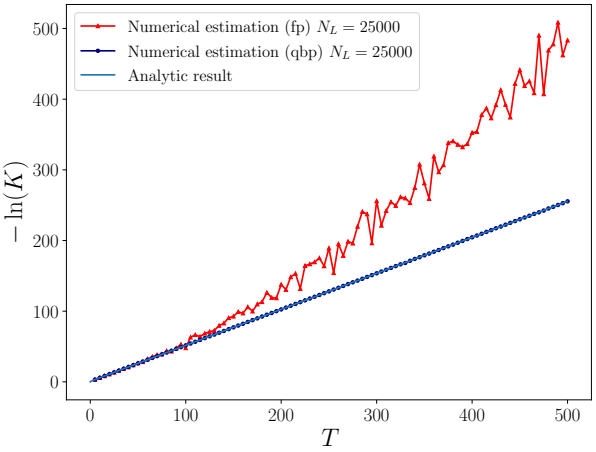

FIG. 5. Estimation of the propagator for the absolute value potential, with $\kappa = 0.5$, and $m = 1$, $\Omega = 0.75$, using $N_L = 25000$ trajectories generated in a harmonic oscillator background with the potential subtraction method (navy) and $N_p = 5000$ points per loop. The blue solid line represent the analytical result based on truncating the spectral representation. The red line with triangles is a estimation using free trajectories.

II. APPLICATIONS

We provide additional information on numerical simulation for the absolute value potential, $V_\kappa(x) = \kappa|x|$. In this case the propagator is not known in closed form, but its spectral representation can be determined from the Hamiltonian's eigenfunctions and energy eigenvalues (the Green function for this system is given in [3]). The eigenfunctions are Airy "Ai" functions, defined for $x \geqslant 0$ as $\Psi_n(x) = c_n \,\mathrm{Ai}\big((2mk)^{\frac{1}{3}}\big(x - \frac{E_n}{k}\big)\big)$ extended symmetrically (anti-symmetrically) for n even (odd). Their energies are written in terms of zeros of the Airy function and its derivative:

$$-E_n = \left(\frac{k^2}{2m}\right)^{\frac{1}{3}} \begin{cases} \tilde{\sigma}_{\frac{n+2}{2}} & n \text{ even} \\ \bar{\sigma}_{\frac{n+1}{2}} & n \text{ odd} \end{cases}, \tag{4}$$

where the $\bar{\sigma}_n$ denote the zeros of Ai and the $\tilde{\sigma}_n$ are the zeros of its derivative, Ai' (all lying along the negative real axis). The normalisation constants, c_n, can be calculated numerically. Truncating the spectral representation provides a good estimate of the kernel for moderate values of propagation time and, in the limit of large times, the ground state, energy $E_0 = -\left(\frac{k^2}{2m}\right)^{\frac{1}{3}}\tilde{\sigma}_1 \approx 1.01879\left(\frac{k^2}{2m}\right)^{\frac{1}{3}}$, dominates according to the asymptotic formula in equation (10) of the Main Text.

This system was simulated using a harmonic oscillator background ($\Omega = 0.75$), fixing $m = 1$, $\kappa = 0.5$, for which the ground state energy is $E_0 = 0.509396\ldots$). This numerical determination of the kernel is shown in Fig 5. Through the linear fit [shown on the graph!] for $T \in [5, 30]$, the energy is estimated to be $E_0 = 0.50939336$.

[1] J. P. Edwards, U. Gerber, C. Schubert, M. A. Trejo, and A. Weber, Integral transforms of the quantum mechanical path integral: hit function and path averaged potential, Phys. Rev. E **97**, 042114 (2018), arXiv:1709.04984 [quant-ph].
[2] J. P. Edwards, U. Gerber, C. Schubert, M. A. Trejo, T. Tsiftsi, and A. Weber, Applications of the worldline Monte Carlo formalism in quantum mechanics, Annals Phys. **411**, 167966 (2019), arXiv:1903.00536 [quant-ph].
[3] C. Grosche and F. Steiner, *Handbook of Feynman Path Integrals*, Vol. 145 (1998).